

DPAR: Dynamic Patchification for Efficient Autoregressive Visual Generation

Divyansh Srivastava¹ Akshay Mehra^{2,†} Pranav Maneriker^{2,†} Debopam Sanyal² Vishnu Raj²
Vijay Kamarshii² Fan Du² Joshua Kimball²
¹University of California, San Diego ²Dolby Laboratories [†] Equal Contribution



Figure 1. **Autoregressive image generation with DPAR.** (a) We show selected samples from our class-conditional DPAR-384-XL model trained on ImageNet. (b) FID vs FLOPs comparison of DPAR model variants trained on 256x256 and 384x384 Image resolution on ImageNet. DPAR achieves reductions in training FLOPs by upto 40% while improving FID by up to 27.1% relative to baseline models.

Abstract

Decoder-only autoregressive image generation typically relies on fixed-length tokenization schemes whose token counts grow quadratically with resolution, substantially increasing the computational and memory demands of attention. We present **DPAR**, a novel decoder-only autoregressive model that dynamically aggregates image tokens into a variable number of patches for efficient image generation. Our work is the first to demonstrate that next-token prediction entropy from a lightweight and unsupervised autoregressive model provides a reliable criterion for merging tokens into larger patches based on information content. DPAR makes minimal modifications to the standard decoder architecture, ensuring compatibility with multimodal generation frameworks and allocating more compute to generation of high-information image regions. Further, we demonstrate that training with dynamically sized patches yields representations that are robust to patch boundaries, allowing DPAR to scale to larger patch sizes at inference. DPAR reduces token count by 1.81x and 2.06x on Imagenet 256 and 384 generation resolution respectively, leading to a re-

duction of up to 40% FLOPs in training costs. Further, our method exhibits faster convergence and improves FID by up to 27.1% relative to baseline models.

1. Introduction

The large-scale success of autoregressive (AR) decoder-only language models [5, 39, 40, 61, 63] has sparked a growing interest in extending next-token prediction paradigm to image generation, for a seamless integration with language models for unified multimodal generation [4, 11, 58, 64, 65]. Recent works [26, 36, 57, 67] demonstrate that AR approaches can achieve performance comparable to, and in some cases surpass, diffusion models [6, 10, 15, 17, 41, 42, 45, 53–55], which have long dominated the image generation [2, 12, 18–22, 48, 49, 70] landscape. Typical AR image generation methods, including LlamaGen [57], employ VQ-VAE [57, 62] to tokenize images into discrete 2D tokens that are flattened into 1D sequences, followed by next-token prediction training with minimal changes to decoder-only transformer model. However, a fundamental scalability challenge persists: the num-

ber of tokens increases quadratically with image resolution, resulting in a substantial increase in the computational and memory costs of attention. For instance, generating a 256×256 image with a standard 16x downsampling requires generating 256 tokens, whereas a 1024×1024 image requires 4096 tokens — a 16x increase in token count and context length for attention.

Existing methods have attempted to reduce token counts for AR image generation through 1D tokenization [8, 31, 51, 69] and token compression techniques [13, 30]. While 1D tokenizers reduce the number of tokens, they are often not favoured due to the loss of 2D spatial structure, which is essential for zero-shot editing capabilities such as extrapolation and outpainting [36]. Moreover, tokens compression methods typically merge statically by a fixed factor, often combining high-information regions, leading to information loss and degraded generation quality. In this work, we ask the question: *Can we dynamically merge tokens based on their information content while preserving the 2D spatial structure for efficient AR image generation?*

To this end, we propose **DPAR**, a novel autoregressive image generation model that dynamically aggregates discrete 2D image tokens into a variable number of *patches* for efficient generation. Images often contain low-information regions such as homogeneous areas like sky or walls that can be represented with fewer tokens without information loss. Inspired by recent advances in the natural language domain [32–34], we propose to leverage next-token prediction entropy from a lightweight and unsupervised AR model as a criterion of information content and merge them into larger units called *patch* (see Figure 2). This allows merging tokens in low-information regions while preserving tokens-level granularity in high-information areas, resulting in a more balanced allocation of compute during generation. Overall, our method unifies the strengths of 2D tokenization, 1D tokenization, and token-merging approaches by preserving 2D spatial structure while dynamically merging tokens based on their information content.

Our method leverages a lightweight encoder that aggregates tokens into patches based on next-token prediction entropy, and a corresponding decoder that reconstructs tokens from generated patches. The autoregressive transformer operates on reduced number of patches instead of tokens, lowering the computational cost of attention. We evaluate our proposed method on ImageNet-256 class-conditional image generation benchmark and demonstrate that DPAR achieves a 1.81x and 2.06x reduction in token count for 256×256 and 384×384 image generation, respectively, leading to a significant reduction of up to 40% GFLOPs in training costs and improves FID by up to 27.1% relative to baselines. Finally, we show that DPAR’s training with a dynamic patch-based representation yields robust representations, enabling DPAR to scale to larger patch sizes at inference. Our con-

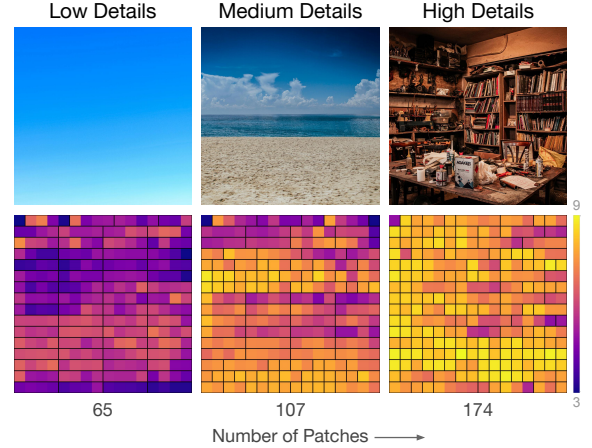


Figure 2. Images (first row) and their corresponding next-token prediction entropy maps (second row) with increasing information content. Images with lower information content produce fewer high-entropy tokens, allowing the model to merge them into larger patches for efficient AR generation. Entropy heatmaps are computed over 256 tokens for 256×256 images, with black outlines indicating the final patch boundaries.

tributions are summarized below:

- We present **DPAR**, a novel autoregressive image generation model that dynamically aggregates image tokens into a variable number of patches based on their information content, enabling efficient generation.
- DPAR achieves 1.81x and 2.06x reduction in token count on ImageNet 256×256 and 384×384 generation, respectively, leading to a significant reduction of up to 40% GFLOPs in training costs. Further, our method exhibits faster convergence and improves FID by up to 27.1% relative to baseline models.
- We demonstrate that DPAR’s training with dynamically-sized patches makes its learned representations robust to patch boundaries. This enables DPAR to scale to larger patch sizes for further efficiency gains during inference.

2. Related Work

Autoregressive Image Generation Seminal work LlamaGen [57] adopts a decoder-only Llama [61] architecture and is trained with standard next-token prediction (NTP) loss on discrete 2D VQ-VAE [62] tokens rasterized left-to-right to 1D sequence, achieving performance comparable to diffusion models [6, 10, 15, 17, 41, 42, 45, 53–55]. Later works have proposed improvements to vanilla AR image generation along two major directions: i) **Random-order Generation** RAR [67] modifies standard NTP training by randomly reordering the raster-order sequence and then linearly lowers the reordering probability, guiding training back to raster order NTP. RandAR [36] removes the raster-order sequencing of decoder-only models and gener-

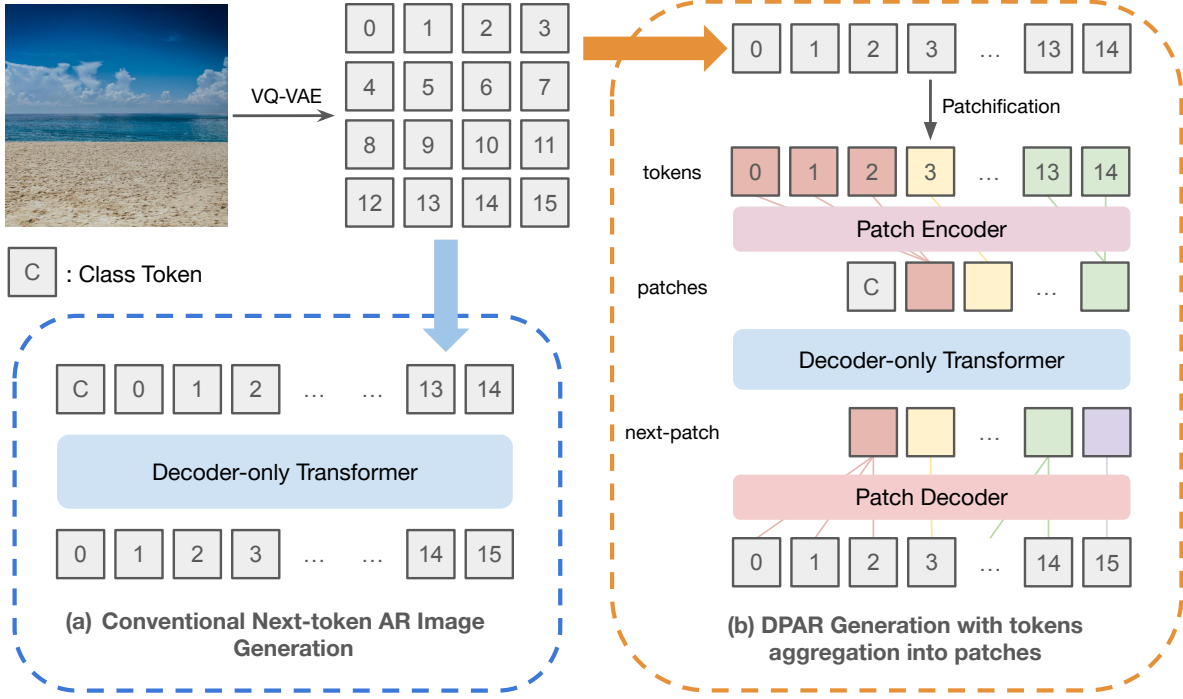


Figure 3. **Overview of DPAR.** (a) Conventional AR image generation employs decoder-only transformers operating on a fixed number of tokens per image, where the token count increases quadratically with image resolution. (b) DPAR dynamically aggregates image tokens based on information content, generating a variable number of patches per image. Decoder-only transformers then operate on a smaller number of patches, reducing computational and memory overhead. DPAR makes minimal modifications to the standard decoder architecture, ensuring compatibility with multimodal generation frameworks.

ates images via random-order next-token prediction, both during training and inference. SAR [27] proposes next-set generation, which is obtained by splitting the sequence into arbitrary sets of multiple tokens. ii) **Modified Training Paradigms** VAR [60] trains a multi-scale tokenizer and generates images by autoregressively producing next-resolution token maps, progressing from coarse to fine resolutions with parallel decoding within each scale step. NPP [35] starts training with large static patches and gradually transitions to standard NTP, and does not use patches at inference time, unlike our method. While these approaches focus on improving the fidelity of AR Image Generation, our work addresses the scalability challenge arising from quadratic token growth in 2D tokenizers with increasing resolution. Further, our approach is orthogonal and complementary to these works and can be combined for further improvements, and we leave this exploration to future work.

Token Reduction for Natural Language Processing Tokenization of text forms a fundamental part of the pipeline for processing text data used in training models for processing natural language. Despite known limitations [1, 46], algorithms utilizing count-based merging of text units called subwords are present in the majority of Large Language

Models (LLMs) today [52]. The most common of these are the Byte Pair Encoding (BPE) [50] tokenizer, which starts by treating each word as a sequence of characters and iteratively merges the most frequent adjacent pair to create larger tokens. Recently, Byte Latent Transformer (BLT) [34] introduced a dynamic byte merging strategy based on next-byte prediction entropy from a lightweight autoregressive model, effectively reducing token count for efficient language modeling starting from bytes. Our work takes inspiration from BLT but unlike BLT which tokenizes text bytes, we demonstrate that next-token prediction entropy can be applied at the VQ-VAE token level to merge low-information spatial tokens into larger patches for efficient autoregressive image generation.

Token Reduction for Image Generation Recent works have explored 1D tokenizers, which aim for better compression ratios and fewer tokens at the expense of 2D spatial structure: CAT [51] primarily focuses on continuous latent space and adjusts token counts from a fixed set of compression ratios (typically 3) predicted by LLM based on the image complexity. TiTok [68] directly compresses images into 1D latent sequences and shows successful representation of 256x256 images with just 32 tokens. One-D-Piece [31] ex-

tends TiTok and proposes tail-token drop to concentrate information at the head of the sequence, allowing for variable length representation. Adaptive Length Image Tokenization [8] recurrently distills 2D discrete tokens into 1D tokens, with each iteration adding more tokens and representation capability. While 1D tokenizers result in fewer tokens, they are often less favored due to the loss of spatial structure, which is crucial for zero-shot editing capabilities such as outpainting and inpainting. Another line of work [13, 30] focuses on token merging techniques to reduce token count: Token-Shuffle [30] leverages the low dimensionality of visual codes to merge local tokens along the channel dimension, effectively reducing the overall token count. However, these methods rely on fixed-scale merging, which can combine high-information regions and result in the loss of fine details during generation. In contrast, our approach combines the strengths of both directions: it supports variable length representations, as in 1D tokenizers, based on image information content, while retaining the 2D spatial structure needed for zero-shot editing tasks.

3. Methodology

3.1. Preliminaries

Autoregressive Image Generation Decoder-only autoregressive models represent an image $I \in \mathbb{R}^{H \times W \times 3}$ as a sequence of discrete 1D tokens and predict each token sequentially, conditioned on the previous tokens. Formally, given an image-condition pair $(I, C) \in \mathcal{D}$ and its tokenized representation $I_{\text{tok}} = [x_0, x_1, \dots, x_{T-1}]$, where $x_i \in \{0, 1, \dots, V-1\}$ is the i^{th} token in an ordered sequence from a vocabulary of size V and T is the total number of tokens. The model learns the likelihood of I as a product of autoregressive factors:

$$P(I_{\text{tok}} \mid C) = \prod_{t=0}^{T-1} P_{\theta}(x_t \mid C, x_{<t}), \quad (1)$$

where C denotes an optional conditioning signal (e.g., class label or text prompt), and P_{θ} is parameterized by a decoder-only transformer with parameters θ . The model is trained to minimize the cross-entropy loss between the predicted next-token probabilities $\hat{P}_{I_{\text{tok}}} = [\hat{p}_0, \dots, \hat{p}_{T-1}]$, where $\hat{p}_t = P_{\theta}(\cdot \mid C, x_{<t})$ and the ground-truth tokens I_{tok} .

$$\mathcal{L}_{CE} = - \sum_{t=0}^{T-1} \log \hat{p}_t(x_t). \quad (2)$$

At inference, model generates images by sampling tokens sequentially from the learned distribution until token length T is reached.

Tokenization One popular choice for image tokenization is VQ-VAE which encodes images into discrete 2D grid of

tokens. Formally, given an image $I \in \mathbb{R}^{H \times W \times 3}$, VQ-VAE downsamples images by a factor of K and maps each latent to a discrete token x_i in the codebook of size V , i.e. $x_i \in \{0, 1, \dots, V-1\}$, resulting in a total of $T = \lceil \frac{H}{K} \rceil \times \lceil \frac{W}{K} \rceil$ tokens. The tokenized 1D sequence is obtained by raster-scanning the 2D tokens from top-left to bottom-right. While this approach has shown promising results in generating high-fidelity images, it suffers from scalability issues as the number of tokens T increases quadratically with image resolution. For instance, increasing the image resolution from 256px to 1024px results in a $16 \times$ increase in the number of tokens, substantially increasing the computational and memory demands of attention in decoder-only AR models. DPAR aims to address quadratic-increase in token count by dynamically merging low-information tokens into patches with simple encoder-decoder modules, leading to efficient AR image generation.

3.2. Dynamic Patchification for Efficient Autoregressive Image Generation

DPAR dynamically aggregates discrete 1D token sequences into a variable length *patch* sequence based on image information content for efficient generation. Our method comprises four main components: (1) a lightweight entropy model that computes next-token prediction entropy for tokens; (2) a patch encoder that aggregates tokens within the same patch into a patch representation of the same dimensionality as each token; (3) a decoder-only transformer that operates on patch representations for efficient autoregressive generation; and (4) a patch decoder that reconstructs individual tokens from the generated patches. We use uppercase symbols to denote sequences or hyperparameters and lowercase symbols to denote individual tokens or scalar values. Figure 3 provides an overview of our method.

3.2.1. Patchification

The goal of patchification is to assign each token in the 1D sequence $I_{\text{tok}} = [x_0, \dots, x_{T-1}]$ to a patch index such that all token indices within a patch remain contiguous. Formally, we construct a patch sequence $I_{\text{patch}} = [P_0, \dots, P_{M-1}]$, where each patch $P_m = [s_m, \dots, e_m]$ is a contiguous non-overlapping span of token indices starting at s_m and ending at e_m in the original token sequence. The number of patches M varies per image and is strictly smaller than the total token count T .

Inspired by BLT [34], we propose to use next-token prediction entropy as a measure of information content for patch formation. We train a lightweight *unconditional* GPT-style AR model with $C = \emptyset$ following Eqs. (1) and (2) and refer to this model as the *entropy model* \mathcal{E}_{ϕ} parameterized by ϕ . We set the next-token prediction entropy for first token, $e_0 = \infty$ to ensure it starts a new patch. The next-token prediction entropy for the token $i \in [1, T-1]$ is computed

Algorithm 1 DPAR Training Algorithm

Input: Image tokens $I_{\text{tok}} = [x_0, \dots, x_{T-1}]$, condition C , entropy model \mathcal{E}_ϕ , threshold E_{Th} , max patch length P_{max}

Output: Cross-entropy loss \mathcal{L}_{CE}

- 1: $I_{\text{patch}} \leftarrow \text{PATCHIFY}(I_{\text{tok}}, 0:T-2, \mathcal{E}_\phi, E_{\text{Th}}, P_{\text{max}})$
- 2: $H_{I_{\text{tok}}}, H_{I_{\text{patch}}} \leftarrow \text{ENCODER}(I_{\text{tok}}, 0:T-2, I_{\text{patch}})$
- 3: $\hat{H}_{I_{\text{patch}}} \leftarrow \text{GPT}(C, H_{I_{\text{patch}}})$ \triangleright AR on patches
- 4: $\hat{P}_{I_{\text{tok}}} \leftarrow \text{DECODER}(H_{I_{\text{tok}}}, \hat{H}_{I_{\text{patch}}})$
- 5: $\mathcal{L}_{\text{CE}} \leftarrow \text{CROSSENTROPYLOSS}(\hat{P}_{I_{\text{tok}}}, I_{\text{tok}})$
- 6: **return** \mathcal{L}_{CE}

Algorithm 2 DPAR Inference Algorithm

Input: Condition C , entropy model \mathcal{E}_ϕ , threshold E_{Th} , max patch length P_{max} , target token length T

Output: Generated image tokens I_{tok}

- 1: $I_{\text{tok}} \leftarrow []$
- 2: **for** $t = 0$ to $T - 1$ **do**
- 3: $I_{\text{patch}} \leftarrow \text{PATCHIFY}(I_{\text{tok}}, \mathcal{E}_\phi, E_{\text{Th}}, P_{\text{max}})$
- 4: $e_t \leftarrow \text{ENTROPY}(x_{<t}, \mathcal{E}_\phi)$
- 5: **if** $e_t \leq E_{\text{Th}}$ **and** $|p_m| < P_{\text{max}}$ **then**
- 6: $H_{I_{\text{tok}}}, - \leftarrow \text{ENCODER}(I_{\text{tok}}, I_{\text{patch}})$
- 7: **else**
- 8: $H_{I_{\text{tok}}}, H_{I_{\text{patch}}} \leftarrow \text{ENCODER}(I_{\text{tok}}, I_{\text{patch}})$
- 9: $\hat{H}_{I_{\text{patch}}} \leftarrow \text{GPT}(C, H_{I_{\text{patch}}})$ \triangleright next-patch
- 10: **end if**
- 11: $\hat{P}_{I_{\text{tok}}} \leftarrow \text{DECODER}(H_{I_{\text{tok}}}, \hat{H}_{I_{\text{patch}}})$
- 12: $x_t \sim \hat{P}_{I_{\text{tok}}}$
- 13: $I_{\text{tok}} \leftarrow I_{\text{tok}} \cup [x_t]$
- 14: **end for**
- 15: **return** I_{tok}

as:

$$\begin{aligned} e_i &= \text{ENTROPY}(x_{<i}, \mathcal{E}_\phi) \\ &= - \sum_{c=0}^{V-1} \mathcal{E}_\phi(x_i = c \mid x_{<i}) \log \mathcal{E}_\phi(x_i = c \mid x_{<i}). \end{aligned} \quad (3)$$

and $E_{I_{\text{tok}}} = \text{ENTROPY}(I_{\text{tok}}, \mathcal{E}_\phi) = [e_0, e_1, \dots, e_{T-1}]$ denotes the entropy values for all tokens in the image. We add a token x_i to the current patch P_m if $e_i \leq E_{\text{Th}}$, and start a new patch P_{m+1} when $e_i > E_{\text{Th}}$. We further limit the patch to a maximum length of P_{max} tokens to prevent excessive aggregation that could lead to information loss, and start a new patch at the end of each row to account for discontinuities in image features at row boundaries. E_{Th} and P_{max} are hyperparameters chosen via ablation, and together they determine the average patch length $P_{\text{avg}} = \mathbb{E}[T/M]$ for a given dataset.

3.2.2. Patch Encoder: Tokens to Patches

The encoder is a lightweight module that encodes tokens within each patch into a patch representation and builds upon the BLT [34] local encoder architecture. Each patch

encoder block consists of causal self-attention among tokens with 2D Rotary Positional Embedding (RoPE) [56] for spatial positional encoding:

$$H_{I_{\text{tok}}} = [h_{x_0}, \dots, h_{x_{T-1}}] = \text{ATTN}([h_{x_0}, \dots, h_{x_{T-1}}]) \quad (4)$$

where h_{x_i} is the latent representation of token x_i after self-attention. This is followed by cross-attention [63] with patches as query and tokens as keys/values. Each patch P_m attends exclusively to its corresponding set of tokens with indices from s_m to e_m :

$$h_{P_m} = \text{CrossAttn}(h_{P_m}, [h_{x_{s_m}}, h_{x_{s_m+1}}, \dots, h_{x_{e_m}}]) \quad (5)$$

and overall patch representations can be represented by $H_{I_{\text{patch}}} = [h_{P_0}, h_{P_1}, \dots, h_{P_{M-1}}]$.

3.2.3. Patch Transformer

The patch transformer is a decoder-only model that operates on patch representations conditioned on a class label or prompt token C . By processing patches instead of individual tokens, it substantially reduces the computational cost of attention while remaining the most compute-intensive component of the pipeline. Following LlamaGen [57], we adopt the LLaMA architecture as our autoregressive decoder backbone and follows typical transformer design with causal self-attention and MLP layers. However, unlike standard transformers that operate on tokens and utilize 2D RoPE for positional encoding, our patch transformer employs a Dynamic RoPE mechanism (see Appendix) for encoding patches with variable token lengths.

3.2.4. Patch Decoder: Patches to Tokens

The decoder is a lightweight module that maps patches back to individual tokens, and is inspired by the local decoder architecture in BLT [34]. Each decoder block consists of a copy operation where patches are copied to their corresponding tokens followed by norm and linear projection:

$$h_{x_i} = h_{x_i} + \text{Linear}(\text{Norm}(h_{P_m})), i \in P_m \quad (6)$$

followed by causal self-attention among tokens with 2D RoPE for positional encoding:

$$H_{I_{\text{tok}}} = [h_{x_0}, \dots, h_{x_{T-1}}] = \text{ATTN}([h_{x_0}, \dots, h_{x_{T-1}}]) \quad (7)$$

4. Experiments

4.1. Implementation Details

Tokenizer We use LlamaGen [57] VQ tokenizer trained on ImageNet [44] with codebook size of $V = 16384$ and downsampling of $K = 16$, resulting in $T = 256$ and $T = 576$ tokens for 256×256 and 384×384 image respectively.

Model	Params	Layers			Hidden	Heads
		Enc.	Global T.	Dec.		
DPAR-B	120M	1	8	3	768	12
DPAR-L	352M	1	19	4	1024	16
DPAR-XL	789M	1	30	5	1280	20
DPAR-XXL	1.4B	1	41	6	1536	24

Table 1. **Architectural specifications of DPAR model variants.**

Enc., Global T., and Dec. refer to patch encoder, global transformer, and patch decoder, layers respectively.

Entropy Model We train an unconditional 111M LlamaGen-B on ImageNet using the same training setup as the patch transformer. For 256×256 images, we use $E_{\text{Th}} = 7.8$ and $P_{\text{max}} = 4$, resulting in an average patch length of $P_{\text{avg}} = 1.81$ on ImageNet training dataset. For 384×384 images, we use $E_{\text{Th}} = 7.9$ and $P_{\text{max}} = 4$, resulting in $P_{\text{avg}} = 2.06$.

DPAR Architecture We implement DPAR with minimal modifications on the LlamaGen architecture. Across all DPAR model variants, we use a single-layer encoder, as our ablations did not show any meaningful gains from deeper encoders (see Appendix). We start with 3 decoder layers for the Base model and increase the number of decoder layers at the same rate as the hidden dimensions (i.e., doubling the hidden dimension from 768 to 1536 increases the decoder layers from 3 to 6). Overall, the aim is to keep both the encoder and decoder shallow, so that the majority of the computational budget is allocated to the patch transformer, which operates on variable-length patches, thereby enabling efficient computation. Furthermore, for each variant, we set the number of patch transformer layers to a value such that the total layer count matches that of LlamaGen models of comparable size for a fair comparison. Detailed DPAR architectural specifications are provided in Table 1.

Training and Sampling We train class-conditional DPAR models on ImageNet for resolutions 256×256 and 384×384. Our models are trained on 8xA100 GPUs with a global batch size of 256 for 300 epochs ($\approx 1.5\text{M}$ steps) using AdamW optimizer with a learning rate of 1e-4, weight decay of 0.05, $\beta_1 = 0.9$, $\beta_2 = 0.95$, and gradient clipping of 1.0 with Pytorch DDP. Other settings, including data augmentation, follow LlamaGen [57]. We do not use any learning rate scheduling and maintain a constant learning rate throughout training. We also use classifier-free guidance [16] with a drop probability of 0.1 during training. We also preprocess tokens and entropy values for each image in the dataset to avoid on-the-fly computation during training. Furthermore, since the patch transformer operates on a variable patch sequence, we implement a packed variant of LlamaGen with xformers [25] to efficiently process

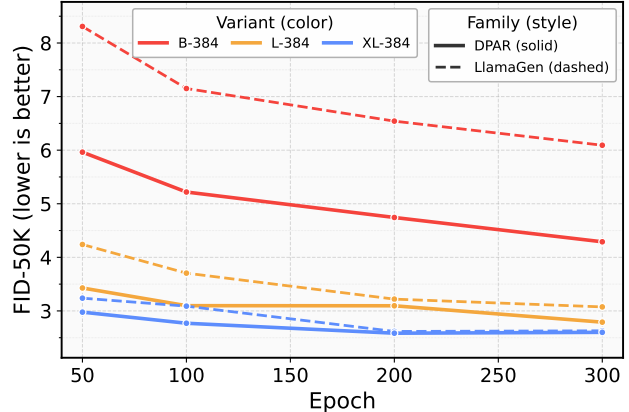


Figure 4. **Comparative analysis of converge of DPAR with LlamaGen on ImageNet-384.** We plot FID vs training epochs for various model sizes. DPAR consistently achieves lower FID scores, demonstrating faster convergence and better image fidelity.

a batch without padding to the maximum sequence length. For sampling, we follow the sampling strategy of LlamaGen [57] and use top-k sampling with $k = 0$, top-p of 1.0, and temperature of 1.0 for all our experiments.

4.2. ImageNet-256 Benchmark

We evaluate the performance of our method on the class-conditional ImageNet-256 generation benchmark, a popular benchmark for image generation [36, 38, 57]. We train class-conditional DPAR model variants on ImageNet at resolutions 256×256 and 384×384 and measure model performance primarily with FID-50K [14], which computes FID between 50,000 generated samples and the ImageNet validation dataset. For 384×384 resolution, the generated images are resized to 256×256 before computing FID, following prior works. We also report Inception Score (IS) [47], and precision/recall [23] for completeness. We primarily compare our model with LlamaGen, as other works either utilize different tokenizers [59], token orderings [27, 36, 67], and training paradigms, making direct comparisons unfair. We leave extending our method to these approaches for future work. Our results are summarized in Table 2. We observe that DPAR outperforms LlamaGen at both resolutions across all model sizes, improving the FID score by as much as 27.10% on the Base model at a 256×256 resolution. We further compare the convergence speed of DPAR and LlamaGen by plotting FID against training epochs in Figure 4 for models trained on resolution 384×384 due to the availability of intermediate epoch results from LlamaGen. We observe that DPAR consistently outperforms LlamaGen throughout training, demonstrating faster convergence and better final performance.

Type	Model	#Params	FID↓	IS↑	Prec.↑	Rec.↑	Steps
Diffusion	ADM [7]	554M	4.59	186.70	0.82	0.523	250
	LDM-4 [43]	400M	3.60	247.70	—	—	250
	DiT-XL [37]	675M	2.27	278.20	0.83	0.57	250
	SiT-XL [29]	675M	2.06	270.30	0.82	0.59	250
Bidirectional AR	MaskGIT-re [3]	227M	4.02	355.60	—	—	8
	MAGVIT-v2 [66]	307M	1.78	319.40	—	—	64
	MAR-L [26]	479M	1.98	290.30	—	—	64
	MAR-H [26]	943M	1.55	303.70	0.81	0.62	256
	TiTok-S-128 [68]	287M	1.97	281.80	—	—	64
Causal AR (non-raster order / modified-training)	VAR [59]	600M	2.57	302.60	0.83	0.56	10
	VAR [59]	2.0B	1.92	350.20	0.82	0.59	10
	SAR-XL [27]	893M	2.76	273.80	0.84	0.55	256
	RAR-L [67]	461M	1.70	299.50	0.81	0.60	256
	RAR-XXL [67]	955M	1.50	306.90	0.80	0.62	256
	RAR-XL [67]	1.5B	1.48	326.00	0.80	0.63	256
	RandAR-L [36]	343M	2.55	288.82	0.81	0.58	88
	RandAR-XL [36]	775M	2.25	317.77	0.80	0.60	88
	RandAR-XXL [36]	775M	2.22	314.21	0.80	0.60	256
	RandAR-XXL [36]	1.4B	2.15	321.97	0.79	0.62	88
Causal AR (raster order)	VQGAN-re [9]	1.4B	5.20	280.30	—	—	256
	RQTran.-re [24]	3.8B	3.80	323.70	—	—	64
	Open-MAGVIT2-XL [28]	1.5B	2.33	271.80	0.84	0.54	256
Causal AR (raster order with LlamaGen tokenizer)	LlamaGen-B [57]	111M	5.46	193.61	0.84	0.46	256
	LlamaGen-L [57]	343M	3.80	248.30	0.83	0.52	256
	LlamaGen-XL [57]	775M	3.39	227.10	0.81	0.54	256
	LlamaGen-384-B [57]	111M	6.09	182.53	0.84	0.42	576
	LlamaGen-384-L [57]	343M	3.07	256.06	0.83	0.52	576
	LlamaGen-384-XL [57]	775M	2.62	244.08	0.80	0.57	576
	DPAR-B (cfg=2.1)	120M	3.98	250.62	0.83	0.49	142
	DPAR-L (cfg=1.9)	352M	2.93	269.34	0.81	0.56	142
	DPAR-XL (cfg=2.0)	789M	2.67	281.65	0.82	0.56	142
	DPAR-384-B (cfg=2.10)	120M	4.29	254.54	0.83	0.47	280
	DPAR-384-L (cfg=1.90)	352M	2.79	283.84	0.81	0.55	280
	DPAR-384-XL (cfg=1.90)	789M	2.60	285.43	0.81	0.57	280

Table 2. **DPAR model comparisons on class-conditional ImageNet 256×256 benchmark.** We report FID [14], Inception Score (IS) [47], and precision/recall [23] and the average number of sampling steps used for generation. DPAR model outperforms prior raster-order autoregressive models with similar parameter counts, achieving significantly better FID scores. Models containing ‘-384’ in their names are trained on 384 × 384 and resized to 256 × 256 for evaluation.

4.3. Training FLOPs

We estimate the mean cost of training by measuring the FLOPs for 500 training steps and averaging the total FLOP measurements over the entire run to obtain a mean per-sample FLOP estimate. This ensures a consistent, profile-based estimate of the end-to-end compute required by DPAR with variable-length patches. The results are summarized in Fig. 1(b). We observe that DPAR significantly reduces training FLOPs across all model sizes compared to LlamaGen, primarily due to the packed implementation of the patch transformer that efficiently handles variable-length patches without padding. Notably, DPAR-XL achieves 40% reduction in training FLOPs compared to LlamaGen-XL on Imagenet 384px generation resolution.

4.4. Ablation Studies

We use DPAR-L model trained on ImageNet 256px resolution for 50 epochs for ablations unless specified otherwise,

and use FID-50K to compare different ablation choices.

Patchification Strategies We consider three binary design choices for patchification: i) starting a new patch when the entropy exceeds a threshold E_{Th} (entropy gating) ii) limiting the maximum patch length to P_{max} (maximum patch length), and iii) resetting patches at row boundaries (row-boundary resets). When all three design choices are disabled, this corresponds to the static patchification scheme with fixed patch length P_{static} , and we set $P_{\text{static}} = 1.81$ to match the average patch length of our full method. The results are summarized in Table 3. We observe that enabling all three design choices leads to the best FID score of 3.32. Furthermore, entropy alone is not sufficient to achieve optimal performance, as the absence of a limit on maximum patch length can lead to excessive aggregation, potentially resulting in information loss.

Entropy	Max Patch Len.	Row Boundary	FID ↓
✗	✗	✗	3.58
✓	✗	✗	3.91
✓	✓	✗	3.45
✓	✓	✓	3.32

Table 3. **Ablation of Patchification strategies.** Entropy-based patchification with patch length constraint and row-boundary resets leads to the best FID score on ImageNet 256×256 benchmark.

E_{Th}	7.6	7.7	7.8	7.9	8.0
FID-50K (↓)	3.36	3.41	3.32	3.46	3.43

Table 4. **Ablation on entropy threshold E_{Th} .** We vary the entropy threshold, keeping the maximum patch length fixed at $P_{\text{max}} = 4$. $E_{\text{Th}} = 7.8$ achieves the best FID of 3.32.

P_{max}	1	2	4	6	8	16
FID-50K (↓)	3.73	3.42	3.32	3.49	3.41	3.61

Table 5. **Ablation on maximum patch length P_{max} .** We vary the maximum patch length, keeping the entropy threshold fixed at $E_{\text{Th}} = 7.8$, with $P_{\text{max}} = 4$, which achieves the best FID of 3.32.

Effect on Entropy Threshold E_{Th} We study the impact of the entropy threshold E_{Th} on FID with a fixed maximum patch length $P_{\text{max}} = 4$ (see Table 4). Lower thresholds produce smaller patches and increase computational cost, whereas higher thresholds produce larger patches but degrade image quality. An intermediate value of $E_{\text{Th}} = 7.8$ provides the best balance, achieving the lowest FID of 3.32.

Effect of Max Patch Length P_{max} We examine the effect of the maximum patch length P_{max} on FID with fixed entropy threshold $E_{\text{Th}} = 7.8$ (see Table 5). We observe that FID first improves as we increase P_{max} from 1 to 4, achieving best FID of 3.32 at $P_{\text{max}} = 4$. However, further increasing P_{max} results in performance degradation, likely due to information loss from excessive aggregation.

4.5. Adaptive Patch Lengths at Inference

We investigate whether DPAR models trained with a fixed entropy threshold E_{Th} can generalize to different entropy thresholds E_{Th} at inference time. To evaluate this, we take our DPAR-L model trained with $E_{\text{Th}} = 7.8$ and $P_{\text{max}} = 4$ for 50 epochs and vary the entropy threshold during inference from 7.8 to 8.1, and compare with static model trained with fixed patch length $P_{\text{static}} = 1.81$ in ablation studies. The results are summarized in Table 6. We observe that as the entropy threshold increases from 7.8 to 8.1, DPAR reduces marginally from 3.32 to 3.39, while the static model’s FID degrades significantly, from 3.58 to 25.59.

E_{Th}	7.8	7.9	8.0	8.1
P_{avg}	1.81	1.92	2.03	2.16
Static	3.58	7.85	17.91	25.59
DPAR-L	3.31	3.32	3.38	3.39

Table 6. **Adaptive Patch Length at Inference.** We compare a static model trained with fixed patch length $P_{\text{static}} = 1.81$ to DPAR-L by varying P_{static} and the entropy threshold E_{Th} respectively at inference. We report the resulting average patch length P_{avg} (2nd row) and set $P_{\text{static}} = P_{\text{avg}}$ for static models. DPAR-L maintains stable FID even as P_{avg} increases from 1.81 to 2.16, whereas the static model exhibits a substantial degradation in FID.

Model	Acc@1	Acc@5
Llamagen-L	32.62	56.61
DPAR-L	37.82	61.15

Table 7. **Linear probing results on ImageNet classification.** We report top-1 and top-5 accuracy (%) on ImageNet validation set using linear probes trained on features extracted from the penultimate layer of our DPAR-L patch transformer and the Llamagen-L.

We argue that DPAR with dynamic patchification leads to learning stronger global representations, as a patch must keep track of future tokens over a variable length. This enables better generalization, resulting in adaptive patch sizes at inference without significant degradation in FID. We further test our hypothesis by linearly probing the last hidden features of DPAR-L patch transformer and LlamaGen-L transformer layers, and average pool patch/token representations to obtain global image features. As shown in Table 7, DPAR features achieve a 5 pp. improvement in both top-1 and top-5 accuracy compared to LlamaGen features, suggesting that DPAR learns better global features.

5. Conclusion

In this work, we introduced DPAR, a novel autoregressive image generation model that dynamically aggregates discrete 2D image tokens into a variable number of patches based on next-token prediction entropy for efficient image generation. Our experiments on ImageNet-1K class-conditional image generation demonstrate that DPAR achieves a significant 2.06x reduction in token count at 384x384 resolution, leading to up to 40% reduction in training FLOPs. We also demonstrate that DPAR exhibits faster convergence and improves FID by up to 27.1% relative to baseline models. Further, training with dynamically sized patches yields representations that are robust to patch boundaries, allowing DPAR to scale to larger patch sizes at inference. While this work focuses on raster-order generation, our proposed strategy is compatible with random-order methods [36, 67] and we plan to explore this in future.

References

[1] Kaj Bostrom and Greg Durrett. Byte pair encoding is sub-optimal for language model pretraining. In *Findings of the Association for Computational Linguistics: EMNLP 2020*, pages 4617–4624, 2020. 3

[2] Andrew Brock, Jeff Donahue, and Karen Simonyan. Large scale gan training for high fidelity natural image synthesis. *arXiv preprint arXiv:1809.11096*, 2018. 1

[3] Huiwen Chang, Han Zhang, Lu Jiang, Ce Liu, and William T Freeman. Maskgit: Masked generative image transformer. In *CVPR*, 2022. 7

[4] Chaorui Deng, Deyao Zhu, Kunchang Li, Chenhui Gou, Feng Li, Zeyu Wang, Shu Zhong, Weihao Yu, Xiaonan Nie, Ziang Song, Guang Shi, and Haoqi Fan. Emerging properties in unified multimodal pretraining, 2025. 1

[5] Jacob Devlin, Ming-Wei Chang, Kenton Lee, and Kristina Toutanova. Bert: Pre-training of deep bidirectional transformers for language understanding. *arXiv preprint arXiv:1810.04805*, 2018. 1

[6] Prafulla Dhariwal and Alexander Nichol. Diffusion models beat gans on image synthesis. *Advances in neural information processing systems*, 34:8780–8794, 2021. 1, 2

[7] Prafulla Dhariwal and Alexander Nichol. Diffusion models beat gans on image synthesis. In *NeurIPS*, 2021. 7

[8] Shivam Duggal, Phillip Isola, Antonio Torralba, and William T Freeman. Adaptive length image tokenization via recurrent allocation. In *First Workshop on Scalable Optimization for Efficient and Adaptive Foundation Models*, 2024. 2, 4

[9] Patrick Esser, Robin Rombach, and Bjorn Ommer. Taming transformers for high-resolution image synthesis. In *CVPR*, 2021. 7

[10] Patrick Esser, Sumith Kulal, Andreas Blattmann, Rahim Entezari, Jonas Müller, Harry Saini, Yam Levi, Dominik Lorenz, Axel Sauer, Frederic Boesel, Dustin Podell, Tim Dockhorn, Zion English, Kyle Lacey, Alex Goodwin, Yanik Marek, and Robin Rombach. Scaling rectified flow transformers for high-resolution image synthesis, 2024. 1, 2

[11] Yuying Ge, Yixiao Ge, Ziyun Zeng, Xintao Wang, and Ying Shan. Planting a seed of vision in large language model, 2023. 1

[12] Ian Goodfellow, Jean Pouget-Abadie, Mehdi Mirza, Bing Xu, David Warde-Farley, Sherjil Ozair, Aaron Courville, and Yoshua Bengio. Generative adversarial nets. *Advances in neural information processing systems*, 27, 2014. 1

[13] Jakob Drachmann Havtorn, Amélie Royer, Tijmen Blankevoort, and Babak Ehteshami Bejnordi. Msvit: Dynamic mixed-scale tokenization for vision transformers. In *Proceedings of the IEEE/CVF International Conference on Computer Vision*, pages 838–848, 2023. 2, 4

[14] Martin Heusel, Hubert Ramsauer, Thomas Unterthiner, Bernhard Nessler, and Sepp Hochreiter. Gans trained by a two time-scale update rule converge to a local nash equilibrium, 2018. 6, 7

[15] Jonathan Ho and Tim Salimans. Classifier-free diffusion guidance. *arXiv preprint arXiv:2207.12598*, 2022. 1, 2

[16] Jonathan Ho and Tim Salimans. Classifier-free diffusion guidance, 2022. 6

[17] Jonathan Ho, Ajay Jain, and Pieter Abbeel. Denoising diffusion probabilistic models. *Advances in neural information processing systems*, 33:6840–6851, 2020. 1, 2

[18] Phillip Isola, Jun-Yan Zhu, Tinghui Zhou, and Alexei A Efros. Image-to-image translation with conditional adversarial networks. In *Proceedings of the IEEE conference on computer vision and pattern recognition*, pages 1125–1134, 2017. 1

[19] Minguk Kang, Jun-Yan Zhu, Richard Zhang, Jaesik Park, Eli Shechtman, Sylvain Paris, and Taesung Park. Scaling up gans for text-to-image synthesis. In *Proceedings of the IEEE/CVF Conference on Computer Vision and Pattern Recognition*, pages 10124–10134, 2023.

[20] Tero Karras, Samuli Laine, and Timo Aila. A style-based generator architecture for generative adversarial networks. In *Proceedings of the IEEE/CVF conference on computer vision and pattern recognition*, pages 4401–4410, 2019.

[21] Tero Karras, Samuli Laine, Miika Aittala, Janne Hellsten, Jaakko Lehtinen, and Timo Aila. Analyzing and improving the image quality of stylegan. In *Proceedings of the IEEE/CVF conference on computer vision and pattern recognition*, pages 8110–8119, 2020.

[22] Tero Karras, Miika Aittala, Samuli Laine, Erik Härkönen, Janne Hellsten, Jaakko Lehtinen, and Timo Aila. Alias-free generative adversarial networks. *Advances in Neural Information Processing Systems*, 34:852–863, 2021. 1

[23] Tuomas Kynkänniemi, Tero Karras, Samuli Laine, Jaakko Lehtinen, and Timo Aila. Improved precision and recall metric for assessing generative models. *Advances in neural information processing systems*, 32, 2019. 6, 7

[24] Doyup Lee, Chiheon Kim, Saehoon Kim, Minsu Cho, and Wook-Shin Han. Autoregressive image generation using residual quantization. In *CVPR*, 2022. 7

[25] Benjamin Lefauveaux, Francisco Massa, Diana Liskovich, Wenhan Xiong, Vittorio Caggiano, Sean Naren, Min Xu, Jieru Hu, Marta Tintore, Susan Zhang, Patrick Labatut, Daniel Haziza, Luca Wehrstedt, Jeremy Reizenstein, and Grigory Sizov. xformers: A modular and hackable transformer modelling library. <https://github.com/facebookresearch/xformers>, 2022. 6

[26] Tianhong Li, Yonglong Tian, He Li, Mingyang Deng, and Kaiming He. Autoregressive image generation without vector quantization. *Advances in Neural Information Processing Systems*, 37:56424–56445, 2024. 1, 7

[27] Wenze Liu, Le Zhuo, Yi Xin, Sheng Xia, Peng Gao, and Xiangyu Yue. Customize your visual autoregressive recipe with set autoregressive modeling. *arXiv preprint arXiv:2410.10511*, 2024. 3, 6, 7

[28] Zhuoyan Luo, Fengyuan Shi, Yixiao Ge, Yujiu Yang, Limin Wang, and Ying Shan. Open-magvit2: An open-source project toward democratizing auto-regressive visual generation. *arXiv preprint arXiv:2409.04410*, 2024. 7

[29] Nanye Ma, Mark Goldstein, Michael S Albergo, Nicholas M Boffi, Eric Vanden-Eijnden, and Saining Xie. SIT: Exploring flow and diffusion-based generative models with scalable

interpolant transformers. *arXiv preprint arXiv:2401.08740*, 2024. 7

[30] Xu Ma, Peize Sun, Haoyu Ma, Hao Tang, Chih-Yao Ma, Jialiang Wang, Kunpeng Li, Xiaoliang Dai, Yujun Shi, Xuan Ju, et al. Token-shuffle: Towards high-resolution image generation with autoregressive models. *arXiv preprint arXiv:2504.17789*, 2025. 2, 4

[31] Keita Miwa, Kento Sasaki, Hidehisa Arai, Tsubasa Takahashi, and Yu Yamaguchi. One-d-piece: Image tokenizer meets quality-controllable compression, 2025. 2, 3

[32] Piotr Nawrot, Jan Chorowski, Adrian Łancucki, and Edoardo M Ponti. Efficient transformers with dynamic token pooling. 2

[33] Piotr Nawrot, Szymon Tworkowski, Michał Tyrołski, Łukasz Kaiser, Yuhuai Wu, Christian Szegedy, and Henryk Michalewski. Hierarchical transformers are more efficient language models, 2022.

[34] Artidoro Pagnoni, Ram Pasunuru, Pedro Rodriguez, John Nguyen, Benjamin Muller, Margaret Li, Chunting Zhou, Lili Yu, Jason Weston, Luke Zettlemoyer, Gargi Ghosh, Mike Lewis, Ari Holtzman, and Srinivasan Iyer. Byte latent transformer: Patches scale better than tokens, 2024. 2, 3, 4, 5

[35] Yatian Pang, Peng Jin, Shuo Yang, Bin Lin, Bin Zhu, Zhenyu Tang, Liuhan Chen, Francis E. H. Tay, Ser-Nam Lim, Harry Yang, and Li Yuan. Next patch prediction for autoregressive visual generation, 2025. 3

[36] Ziqi Pang, Tianyuan Zhang, Fujun Luan, Yunze Man, Hao Tan, Kai Zhang, William T Freeman, and Yu-Xiong Wang. Randar: Decoder-only autoregressive visual generation in random orders. In *Proceedings of the Computer Vision and Pattern Recognition Conference*, pages 45–55, 2025. 1, 2, 6, 7, 8

[37] William Peebles and Saining Xie. Scalable diffusion models with transformers. In *ICCV*, 2023. 7

[38] William Peebles and Saining Xie. Scalable diffusion models with transformers, 2023. 6

[39] Alec Radford, Karthik Narasimhan, Tim Salimans, Ilya Sutskever, et al. Improving language understanding by generative pre-training. *article*, 2018. 1

[40] Colin Raffel, Noam Shazeer, Adam Roberts, Katherine Lee, Sharan Narang, Michael Matena, Yanqi Zhou, Wei Li, and Peter J Liu. Exploring the limits of transfer learning with a unified text-to-text transformer. *The Journal of Machine Learning Research*, 21(1):5485–5551, 2020. 1

[41] Aditya Ramesh, Prafulla Dhariwal, Alex Nichol, Casey Chu, and Mark Chen. Hierarchical text-conditional image generation with clip latents. *arXiv preprint arXiv:2204.06125*, 1 (2):3, 2022. 1, 2

[42] Robin Rombach, Andreas Blattmann, Dominik Lorenz, Patrick Esser, and Björn Ommer. High-resolution image synthesis with latent diffusion models. In *Proceedings of the IEEE/CVF conference on computer vision and pattern recognition*, pages 10684–10695, 2022. 1, 2

[43] Robin Rombach, Andreas Blattmann, Dominik Lorenz, Patrick Esser, and Björn Ommer. High-resolution image synthesis with latent diffusion models. In *CVPR*, 2022. 7

[44] Olga Russakovsky, Jia Deng, Hao Su, Jonathan Krause, Sanjeev Satheesh, Sean Ma, Zhiheng Huang, Andrej Karpathy, Aditya Khosla, Michael Bernstein, Alexander C. Berg, and Li Fei-Fei. Imagenet large scale visual recognition challenge, 2015. 5

[45] Chitwan Saharia, William Chan, Saurabh Saxena, Lala Li, Jay Whang, Emily L Denton, Kamyar Ghasemipour, Raphael Gontijo Lopes, Burcu Karagol Ayan, Tim Salimans, et al. Photorealistic text-to-image diffusion models with deep language understanding. *Advances in Neural Information Processing Systems*, 35:36479–36494, 2022. 1, 2

[46] Jonne Sälevä and Constantine Lignos. What changes when you randomly choose bpe merge operations? not much. In *Proceedings of the Fourth Workshop on Insights from Negative Results in NLP*, pages 59–66, 2023. 3

[47] Tim Salimans, Ian Goodfellow, Wojciech Zaremba, Vicki Cheung, Alec Radford, and Xi Chen. Improved techniques for training gans, 2016. 6, 7

[48] Axel Sauer, Katja Schwarz, and Andreas Geiger. Styleganxl: Scaling stylegan to large diverse datasets. In *ACM SIGGRAPH 2022 conference proceedings*, pages 1–10, 2022. 1

[49] Axel Sauer, Tero Karras, Samuli Laine, Andreas Geiger, and Timo Aila. Stylegan-t: Unlocking the power of gans for fast large-scale text-to-image synthesis. *arXiv preprint arXiv:2301.09515*, 2023. 1

[50] Rico Sennrich, Barry Haddow, and Alexandra Birch. Neural machine translation of rare words with subword units. In *Proceedings of the 54th annual meeting of the association for computational linguistics (volume 1: long papers)*, pages 1715–1725, 2016. 3

[51] Junhong Shen, Kushal Tirumala, Michihiro Yasunaga, Ishan Misra, Luke Zettlemoyer, Lili Yu, and Chunting Zhou. Cat: Content-adaptive image tokenization. *arXiv preprint arXiv:2501.03120*, 2025. 2, 3

[52] Aaditya K Singh and DJ Strouse. Tokenization counts: the impact of tokenization on arithmetic in frontier llms. *arXiv preprint arXiv:2402.14903*, 2024. 3

[53] Jiaming Song, Chenlin Meng, and Stefano Ermon. Denoising diffusion implicit models. *arXiv preprint arXiv:2010.02502*, 2020. 1, 2

[54] Yang Song and Stefano Ermon. Generative modeling by estimating gradients of the data distribution. *Advances in neural information processing systems*, 32, 2019.

[55] Divyansh Srivastava, Xiang Zhang, He Wen, Chenru Wen, and Zhuowen Tu. Lay-your-scene: Natural scene layout generation with diffusion transformers, 2025. 1, 2

[56] Jianlin Su, Yu Lu, Shengfeng Pan, Ahmed Murtadha, Bo Wen, and Yunfeng Liu. Roformer: Enhanced transformer with rotary position embedding, 2023. 5, 1

[57] Peize Sun, Yi Jiang, Shoufa Chen, Shilong Zhang, Bingyue Peng, Ping Luo, and Zehuan Yuan. Autoregressive model beats diffusion: Llama for scalable image generation. *arXiv preprint arXiv:2406.06525*, 2024. 1, 2, 5, 6, 7

[58] Chameleon Team. Chameleon: Mixed-modal early-fusion foundation models, 2025. 1

[59] Keyu Tian, Yi Jiang, Zehuan Yuan, Bingyue Peng, and Liwei Wang. Visual autoregressive modeling: Scalable image

generation via next-scale prediction. *Advances in neural information processing systems*, 37:84839–84865, 2024. [6](#), [7](#)

[60] Keyu Tian, Yi Jiang, Zehuan Yuan, Bingyue Peng, and Liwei Wang. Visual autoregressive modeling: Scalable image generation via next-scale prediction, 2024. [3](#)

[61] Hugo Touvron, Thibaut Lavril, Gautier Izacard, Xavier Martinet, Marie-Anne Lachaux, Timothée Lacroix, Baptiste Rozière, Naman Goyal, Eric Hambro, Faisal Azhar, et al. Llama: Open and efficient foundation language models. *arXiv preprint arXiv:2302.13971*, 2023. [1](#), [2](#)

[62] Aaron van den Oord, Oriol Vinyals, and Koray Kavukcuoglu. Neural discrete representation learning, 2018. [1](#), [2](#)

[63] Ashish Vaswani, Noam Shazeer, Niki Parmar, Jakob Uszkoreit, Llion Jones, Aidan N Gomez, Łukasz Kaiser, and Illia Polosukhin. Attention is all you need. *Advances in neural information processing systems*, 30, 2017. [1](#), [5](#)

[64] Xinlong Wang, Xiaosong Zhang, Zhengxiong Luo, Quan Sun, Yufeng Cui, Jinsheng Wang, Fan Zhang, Yueze Wang, Zhen Li, Qiying Yu, et al. Emu3: Next-token prediction is all you need. *arXiv preprint arXiv:2409.18869*, 2024. [1](#)

[65] Lili Yu, Bowen Shi, Ramakanth Pasunuru, Benjamin Muller, Olga Golovneva, Tianlu Wang, Arun Babu, Binh Tang, Brian Karrer, Shelly Sheynin, Candace Ross, Adam Polyak, Russell Howes, Vasu Sharma, Puxin Xu, Hovhannes Tamoyan, Oron Ashual, Uriel Singer, Shang-Wen Li, Susan Zhang, Richard James, Gargi Ghosh, Yaniv Taigman, Maryam Fazel-Zarandi, Asli Celikyilmaz, Luke Zettlemoyer, and Armen Aghajanyan. Scaling autoregressive multi-modal models: Pretraining and instruction tuning, 2023. [1](#)

[66] Lijun Yu, José Lezama, Nitesh B. Gundavarapu, Luca Versari, Kihyuk Sohn, David Minnen, Yong Cheng, Vignesh Birodkar, Agrim Gupta, Xiuye Gu, Alexander G. Hauptmann, Boqing Gong, Ming-Hsuan Yang, Irfan Essa, David A. Ross, and Lu Jiang. Language model beats diffusion–tokenizer is key to visual generation. In *ICLR*, 2024. [7](#)

[67] Qihang Yu, Ju He, Xueqing Deng, Xiaohui Shen, and Liang-Chieh Chen. Randomized autoregressive visual generation. *arXiv preprint arXiv:2411.00776*, 2024. [1](#), [2](#), [6](#), [7](#), [8](#)

[68] Qihang Yu, Mark Weber, Xueqing Deng, Xiaohui Shen, Daniel Cremers, and Liang-Chieh Chen. An image is worth 32 tokens for reconstruction and generation. *Advances in Neural Information Processing Systems*, 37:128940–128966, 2024. [3](#), [7](#)

[69] Qihang Yu, Mark Weber, Xueqing Deng, Xiaohui Shen, Daniel Cremers, and Liang-Chieh Chen. An image is worth 32 tokens for reconstruction and generation, 2024. [2](#)

[70] Jun-Yan Zhu, Taesung Park, Phillip Isola, and Alexei A Efros. Unpaired image-to-image translation using cycle-consistent adversarial networks. In *Proceedings of the IEEE international conference on computer vision*, pages 2223–2232, 2017. [1](#)

DPAR: Dynamic Patchification for Efficient Autoregressive Visual Generation

Supplementary Material

6. Training

6.1. Patchification Algorithm

The patchification algorithm assigns each token in the 1D sequence $I_{\text{tok}} = [x_0, \dots, x_{T-1}]$ to a patch index such that all token indices within a patch remain contiguous. Formally, we construct a patch sequence $I_{\text{patch}} = [P_0, \dots, P_{M-1}]$, where each patch $P_m = [s_m, \dots, e_m]$ is a contiguous non-overlapping span of token indices starting at s_m and ending at e_m in the original token sequence. The number of patches M varies per image and is strictly smaller than the total token count T .

Algorithm 3 DPAR Patchification Algorithm

Input: Image tokens $I_{\text{tok}} = [x_0, x_1, \dots, x_{T-1}]$, entropy model \mathcal{E}_ϕ , threshold E_{Th} , max patch length P_{max}

Output: Patch sequence I_{patch}

- 1: $I_{\text{patch}} \leftarrow [[x_0]]$ \triangleright Initialize first patch with first token
- 2: $P \leftarrow [x_1]$ \triangleright Current patch
- 3: **for** $i = 2$ to $T - 1$ **do**
- 4: $e_i \leftarrow \text{ENTROPY}(x_{<i}, \mathcal{E}_\phi)$
- 5: **if** $e_i \leq E_{\text{Th}}$ **and** $|P| < P_{\text{max}}$ **and** x_i not at row start **then**
- 6: $P \leftarrow P \cup [x_i]$ \triangleright Add token to current patch
- 7: **else**
- 8: $I_{\text{patch}} \leftarrow I_{\text{patch}} \cup [P]$ \triangleright Finalize current patch
- 9: $P \leftarrow [x_i]$ \triangleright Start new patch
- 10: **end if**
- 11: **end for**
- 12: $I_{\text{patch}} \leftarrow I_{\text{patch}} \cup [P]$ \triangleright Add last patch
- 13: **return** I_{patch}

6.2. Ablation Study: Encoder-Decoder Layers

We conduct an ablation study to analyze the impact of varying the number of encoder and decoder layers on model performance, keeping the total number of encoder and decoder layers constant. As shown in Table 10, configurations with shallower encoders and deeper decoders (E1D4) yield the best FID scores. This suggests that allocating more capacity to the decoder is beneficial for generating high-quality images, while a lighter encoder suffices for aggregating tokens into patches.

6.3. Dynamic RoPE

2D Rotary Positional Embedding (RoPE) [56] encodes each token's 2D spatial coordinate (x, y) by rotating its query and key representations in latent space with dimensionality d using sinusoidal functions of the coordinates. For a token

Variant	LlamaGen (GFLOPs)	DPAR (GFLOPs)
B-256	24.98	19.21
L-256	83.26	56.74
XL-256	192.69	125.52
B-384	56.21	40.92
L-384	187.35	117.92
XL-384	433.57	258.53

Table 8. **Compute comparison across all LlamaGen and DPAR variants.** DPAR consistently reduces FLOPs across both 256x256 and 384x384 model families.

Method	FID \downarrow
2D Embedding	3.32
Dynamic Embedding w/o redundancy	3.42
Dynamic Embedding	3.31

Table 9. **Comparison of positional embedding schemes.** Dynamic Embedding achieves the best FID on ImageNet 256x256.

Layers (E#D#)	E1D4	E2D3	E3D2	E4D1
FID-50K (↓)	3.32	3.35	3.51	3.85

Table 10. **Ablation on encoder-decoder depth.** $E_i D_j$ indicates i encoder layers and j decoder layers. Shallow encoders with deeper decoders (E1D4) provide the best FID.

located at 2D coordinates (x, y) in the image, the positional encoding is given by:

$$\begin{aligned} \omega_i &= 10000^{-4(i-1)/d}, \quad i = 1, \dots, \frac{d}{4}, \\ P_x &= [\sin(\omega_i x), \cos(\omega_i x)]_{i=1}^{d/4}, \\ P_y &= [\sin(\omega_i y), \cos(\omega_i y)]_{i=1}^{d/4}, \\ P_{(x,y)} &= [P_x, P_y] \end{aligned} \quad (8)$$

where ω_i are the frequency terms, and the resulting $P_{(x,y)}$ is used to rotate the query and key vectors to encode 2D spatial relationships. We propose Dynamic RoPE, an extension of 2D RoPE to handle variable length patches by encoding the start and end coordinates of each patch along the y-axis. This is possible since each row starts a new patch. The updated positional encoding for a patch p_m that spans tokens

from (x, y_{s_m}) to (x, y_{e_m}) is defined as:

$$\begin{aligned}
\omega_i &= 10000^{-4(i-1)/d}, \quad i = 1, \dots, \frac{d}{4}, \\
\alpha_i &= 10000^{-16(i-1)/d}, \quad i = 1, \dots, \frac{d}{16}, \\
P_x &= [\sin(\omega_i x), \cos(\omega_i x)]_{i=1}^{d/4}, \\
P_{y_s} &= [\sin(\alpha_i y_{s_m}), \cos(\alpha_i y_{s_m})]_{i=1}^{d/16}, \\
P_{y_e} &= [\sin(\alpha_i y_{e_m}), \cos(\alpha_i y_{e_m})]_{i=1}^{d/16}, \\
P_{(x, y_s, y_e)} &= [Pos_x, Pos_{y_s}, Pos_{y_e}, Pos_{y_e}, Pos_{y_s}]
\end{aligned} \tag{9}$$

Our idea is to encode both the starting and ending y-coordinates of each patch, allowing the model to capture the horizontal span of each patch in addition to its vertical position. Further, added redundancy by repeating the start and end positional encodings leads to better representation as observed in Table 9.

Model	Params	Epoch	CFG	FID\downarrow	IS\uparrow	Prec.\uparrow	Rec.\uparrow
B-256	120M	300	1.75	5.02	193.99	0.78	0.54
			1.90	4.28	219.40	0.81	0.52
			2.00	4.07	235.39	0.82	0.50
			2.10	3.98	250.62	0.83	0.49
L-256	352M	300	1.75	3.24	241.05	0.79	0.58
			1.90	2.93	269.34	0.81	0.56
			2.00	2.96	284.06	0.82	0.54
			2.10	3.03	298.19	0.83	0.54
XL-256	789M	200	2.00	2.86	277.37	0.82	0.56
			1.75	2.82	249.57	0.79	0.60
		300	1.90	2.69	270.30	0.81	0.57
			2.00	2.67	281.65	0.82	0.56
			2.10	2.73	292.07	0.82	0.56

Table 11. **Comparison of models, parameters, epochs, and CFG values.** for model trained on resolution 256 \times 256

Model	Params	Epoch	CFG	FID↓	IS↑	Prec.↑	Rec.↑
B-384	120M	50	2.00	5.96	190.16	0.79	0.47
		100	2.00	5.22	213.44	0.82	0.46
		200	2.00	4.74	230.43	0.81	0.48
			1.75	5.46	196.58	0.78	0.52
		300	1.90	4.62	223.31	0.81	0.50
			2.00	4.41	237.38	0.82	0.48
			2.10	4.29	254.54	0.83	0.47
L-384	352M	50	2.00	3.43	285.02	0.83	0.52
		100	2.00	3.10	290.11	0.82	0.53
		200	2.00	3.10	298.13	0.82	0.53
			1.75	3.00	256.07	0.79	0.58
		300	1.90	2.79	283.84	0.81	0.55
			2.00	2.84	299.32	0.82	0.55
			2.10	2.93	315.02	0.83	0.54
XL-384	789M	50	2.00	2.98	289.90	0.81	0.55
		100	2.00	2.77	307.30	0.82	0.56
		200	2.00	2.58	308.11	0.83	0.55
			1.75	2.81	261.09	0.79	0.59
		300	1.90	2.60	285.43	0.81	0.57
			2.00	2.62	299.31	0.82	0.57
			2.10	2.68	314.75	0.82	0.56

Table 12. **Comparison of models, parameters, epochs, and CFG values.** for model trained on resolution 384×384



Figure 5. Uncurated generated samples for model **DPAR-XL** trained at 256×256 resolution at **CFG-scale=1.75**



Figure 6. Uncurated generated samples for model **DPAR-XL** trained at 256×256 resolution at **CFG-scale=1.9**

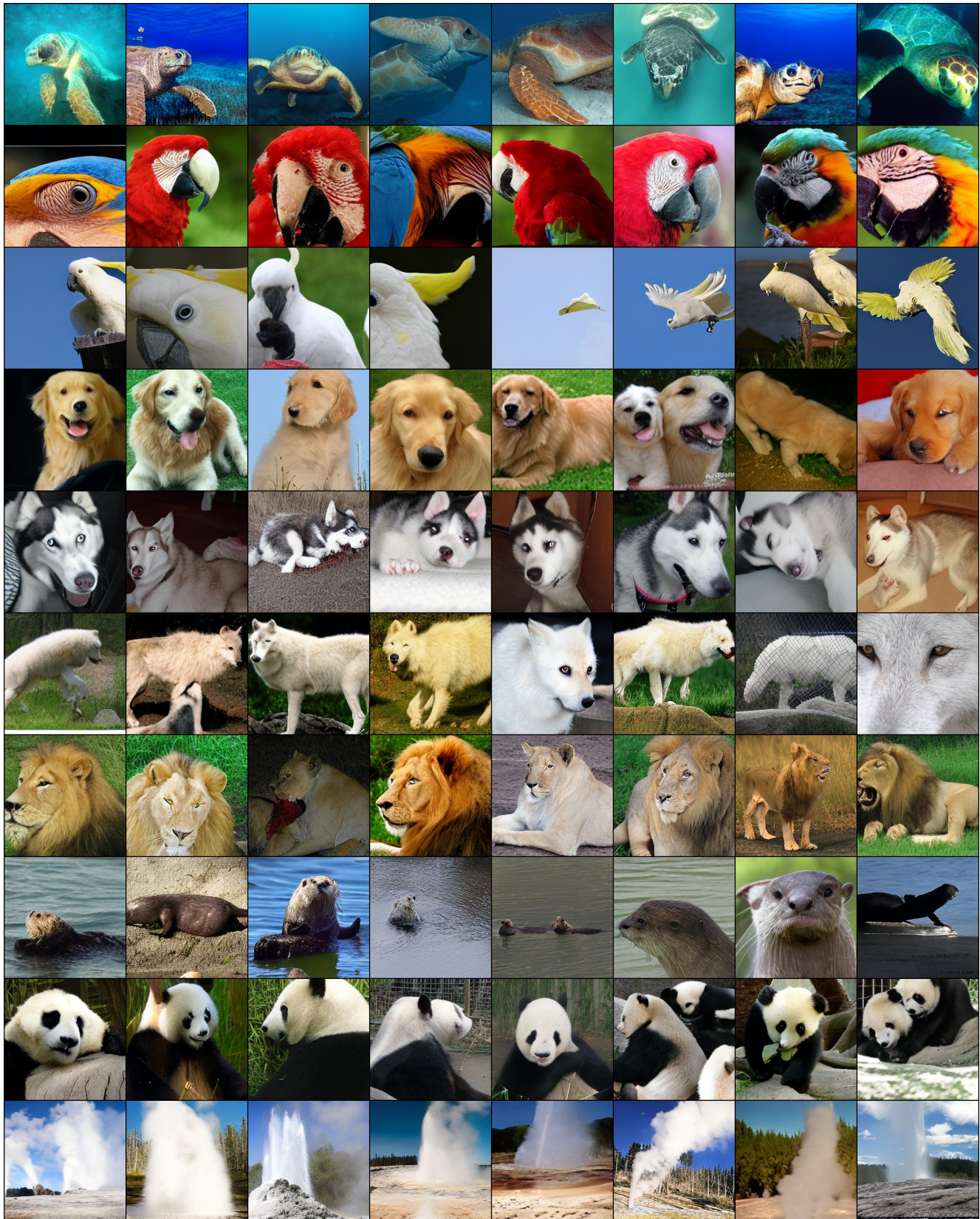


Figure 7. Uncurated generated samples for model **DPAR-XL** trained at 256×256 resolution at **CFG-scale=2.0**



Figure 8. Uncurated generated samples for model **DPAR-XL** trained at 256×256 resolution at **CFG-scale=2.1**



Figure 9. Uncurated generated samples for model **DPAR-XL** trained at 384×384 resolution at **CFG-scale=1.75**



Figure 10. Uncurated generated samples for model **DPAR-XL** trained at 384×384 resolution at **CFG-scale=1.9**



Figure 11. Uncurated generated samples for model **DPAR-XL** trained at 384×384 resolution at **CFG-scale=2.0**



Figure 12. Uncurated generated samples for model **DPAR-XL** trained at 384×384 resolution at **CFG-scale=2.1**